Performance Analysis and Optimal Design of Multichannel Equalizer for Underwater Acoustic Communications

Milutin Pajovic and James C. Preisig

***Abstract*—Adaptive equalization is a widely used method of mitigating the effects of multipath propagation and Doppler spreading in underwater acoustic communication channels. While the structure of a multichannel equalizer and least-squares-based adaptation algorithm are extensively used in practice, little is known in how to choose the number of sensors, separation between them, and lengths of the constituent filters such that the equalization performance is optimized. This paper studies the problem of optimal multichannel equalizer design in the context of time-varying underwater acoustic communication channels. In the first part, the paper presents a theoretical characterization of the equalization performance when the number of symbols that can be received in the time period over which the channel can be considered time invariant is limited. This result is then used to develop an understanding that the optimal number of equalizer coefficients is a tradeoff between the minimum mean squared error (MMSE) requirement for longer constituent filters and the insight that the limit on the number of stationary observations also limits the number of filter coefficients that can be effectively adapted. In the second part, the paper develops a theoretical model for wideband arrivals impinging upon an array of sensors of the multichannel equalizer. This model is used to develop an understanding that the optimal sensor separation is a tradeoff between the requirement for long aperture which improves resolution, and the fact that the grating lobes, caused by spatial undersampling, limit the equalizer's ability to estimate the transmitted signal from the received signal.**

***Index Terms*—Multichannel equalizer, optimal design, performance analysis, underwater acoustic communications.**

I. Introduction

THE wireless communication channels through which signals are transmitted are often time varying and characterized by multipath propagation. The multipath propagation gives rise to a delay spread, resulting in intersymbol interference (ISI) in the received signal, while the time variability results in the Doppler spreading of the signal [1]. These effects are even more profound in the setting of underwater acoustic communications wherein, along with a high latency due to a relatively slow speed of propagation (nominally 1500 m/s) and frequency-dependent attenuation of the transmitted signal, these effects pose significant challenges to communication system design [2].

Different techniques have been developed for mitigating these effects [3]. A survey of the approaches used for the underwater acoustic communication system design is given in [4]. Most techniques rely in part or completely on channel equalization with a decision feedback equalizer (DFE) being the most commonly used form [5]. A multichannel DFE (MC–DFE) is one which processes the signals received at multiple spatially separated sensors. The MC–DFE is particularly effective at compensating for the ISI induced by the multipath commonly present in the underwater acoustic communication channel.

One of the main challenges in optimally configuring a multichannel equalizer is the choice of the number of sensors and lengths of the constituent filters. On the one hand, when the channel impulse response and characteristics of interfering signals including ambient noise are perfectly known such that the minimum mean squared error (MMSE) optimal filter coefficients can be calculated, the MMSE achievable by the equalizer is a monotonically nonincreasing function of the number of sensors and the lengths of the filters. However, in practical scenarios, neither the channel impulse response nor the characteristics of the interfering signals are known and the equalizer filter coefficients must be adapted based upon observations of the received signal. In this case, the time variability of the channel limits the number of observations that can be gathered in an interval over which the channel and noise conditions can be considered roughly stationary, which in turn limits the number of filter coefficients that can be effectively adapted. Therefore, a lower MSE may be achieved using either smaller numbers of sensors and/or lengths of the equalizer filters.

Another challenge related to optimally configuring the mutlichannel equalizer is the selection of separation between sensors. While the sensors in a multiple-input–multiple-output (MIMO) system need to be sufficiently apart so that the signals at their outputs are uncorrelated [6], conventional wisdom is that array processing applications require that sensors be separated by no more than one half of the shortest wavelength of

Manuscript received January 29, 2015; accepted August 11, 2015. Date of publication September 17, 2015; date of current version October 09, 2015. This work was supported in part by the U.S. Office of Naval Research (ONR) under Grants N00014-11-10426, N00014-10-10259, and N00014-07-10738, and Contract N00014-14C-0230; and by the National Science Foundation (NSF) under Grant ECCS-1102156. This work was presented in part at the 2014 Conference on Underwater Communications and Networking (UComms), Sestri Levante, Italy, Sep. 2014.

Associate Editor: M. Stojanovic.

M. Pajovic was with the Massachusetts Institute of Technology and Woods Hole Oceanographic Institution Joint Program, Cambridge/Woods Hole, MA 02139 USA. He is currently with Mitsubishi Electric Research Laboratories, Cambridge, MA 02139 USA (e-mail: pajovic@merl.com).

J. C. Preisig is with JPAnalytics LLC, Falmouth, MA 02540 USA and also with the Department of Applied Ocean Physics and Engineering, Woods Hole Oceanographic Institution, Woods Hole, MA 02543 USA (e-mail: jpreisig@jp-analytics.com).

the received signals [7]. However, in many underwater acoustic channels, the signals arrive from a limited range of vertical angles. When linear vertical arrays are used in such situations, the channel appears sparse in the vertical wave number domain and the selection of the optimal sensor separation is a more subtle problem.

A comprehensive performance study of the MMSE-based equalization, reported in [8] and [9], analyzes how the number of channels and filter taps in a multichannel equalizer impacts the performance. In terms of optimal DFE design, Gong and Cowan [10], [11] discuss how the decision delay, feedforward and feedback filter lengths should be selected such that the signal prediction mean squared error (MSE) of the MMSE-based DFE equalizer of a linear time-invariant (LTI) channel is minimized. However, these works inherently assume that the observation period is infinitely long, which is not the case in nonstationary channels where only a limited number of stationary observations are available for adaptation. In comparison, we study the equalization problem in a setting where the number of stationary observations is finite and often limited, which is particularly the case in underwater acoustic communications. We note that the recent development in asymptotic random matrix theory (RMT) has allowed the impact of a limited observation window to be handled in a reasonably tractable manner.

The structure of the MC–DFE equalizer and MMSE and least squares (LS) algorithms for computing its weights have been introduced in [12]. In addition, Stojanovic *et al.* [12] analytically study the performance of the MMSE-based equalizer and experimentally demonstrate the performance of the LS-based equalizer. Finally, Stojanovic *et al.* [12] present an intuition behind the relationship between beamforming and channel combining for narrowband plane wave arrivals in white ambient noise. In comparison, we analytically study the performance of the LS-based equalizer and by employing a more general arrival model with wideband, spatially spread arrivals in nonisotropic noise, bring into sharper focus the relations between equalization performance, the number of sensors, separation between them, and lengths of the constituent filters.

The issue of noise enhancement, caused when the observation window is not large enough to enable adaptation of the employed number of equalizer taps, is, together with the computational complexity considerations, the main motivation in [13] behind the introduction of a processor which precedes MC–DFE and reduces the number of parallel channel branches that go into the MC–DFE. The experimental demonstration of the proposed scheme reveals that such a receiver might still suffer performance degradation if the overall number of equalizer taps is excessively large. This result further amplifies the necessity to study the noise enhancement effect in the context of the LS-based multichannel equalization of ocean channels.

One of the results of our study indicates that an optimal equalizer may have shorter time span than the delay spread of the acoustic channel when the channel varies such that the effective observation window is short. Short equalizers naturally arise when a possibly sparse structure in the acoustic channel impulse response is exploited such as in [14]. However, our focus is LS-based multichannel equalization such that when optimal equalizer has relatively short constituent filters, it is the result of rapid variations in the ocean channel.

The analytical results addressing the equalization performance in the observation deficient regime (i.e., with LS-based adaptation of weighs) appeared relatively recently.

As such, Xiao and Honig [15] study the signal-to-noise-plus-interference ratio (SINR) at the output of the LS-based linear equalizer for a time-invariant frequency flat-fading channel. A more general analysis in [16] characterizes the SINR at the output of the LS-based linear equalizer for time-invariant frequency-selective channels.

This paper analyzes the equalization performance and explores its dependence on the number of sensors, separation between them, and lengths of the constituent filters when the equalizer operates in a time-varying underwater acoustic communication channel. The contributions of this paper are twofold. First, an analytical characterization of the LS-based MC–DFE equalization performance in time-varying channel is presented. The derived expression quantitatively supports the observed performance characteristic that, when working with signals that have passed through time-varying channels, an equalizer with relatively short constituent filters can outperform one using longer filters [17]. The optimal number of taps in the equalizer's constituent filters is presented as a tradeoff between two competing requirements. On the one hand, for a perfectly known environment, the MMSE error criterion is a nonincreasing function of filter length. On the other hand, the insights from random matrix theory (RMT) imply that for a given number of observation vectors, the shorter constituent filters lead to more accurate estimate of the correlation matrix and therefore improved performance.

Second, the paper analyzes how the number of and separation between the sensors impact the equalization performance in a time-varying underwater acoustic communication channel. Our model for the arrival process takes into account that the underwater acoustic communication signal is wideband and, when received on a vertical array of sensors, sparse in the vertical wave number domain. Using this framework, we illustrate with a particular arrival model that the equalization performance is optimized for a finite sensor separation which is not necessarily equal to one half of the shortest wavelength of the received signal. In addition, we analyze how the array aperture impacts the performance and develop an intuitive understanding of these effects.

The rest of the paper is organized as follows. A background on the MC–DFE which describes its structure, analytical framework, and updating algorithm is given in Section II. The challenges related to optimal multichannel equalizer design are motivated in Section III. Section IV presents the performance analysis of the MC–DFE when adapting using a limited number of observations of the received signal and shows that the number of coefficients which optimizes the equalizer performance is a tradeoff between two competing requirements. The model for sparse, wideband, and spatially spread arrivals, inherent to the

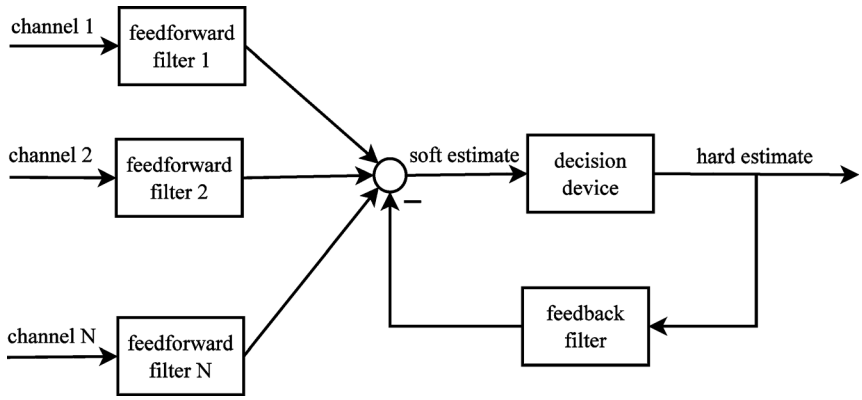

Fig. 1. Block diagram of multichannel decision feedback equalizer [12].

underwater acoustic environment, is presented in Section V. The impact of sensor separation and array aperture on performance of multichannel equalizer is studied in Section VI. Finally, Section VII concludes the paper.

II. Background

The structure of the MC–DFE, analytical framework, and LS-based adaptation algorithm are briefly described in this section.

A. MC–DFE: Structure

The structure of the MC–DFE equalizer is shown in Fig. 1. It contains a feedforward (FF) filter bank, feedback (FB) filter, and a decision device. The FF filter bank consists of one linear filter to process the input from each channel (sensor). A signal received at each sensor is, after some preprocessing such as filtering, sampling, conversion to baseband, and downsampling, further processed by a corresponding FF filter. The ultimate goal of the FF processing is to coherently combine the received signal energy and attenuate ISI and ambient noise signals. In comparison, the linear FB filter processes the equalizer's outputs (i.e., estimates of the transmitted symbols) with the goal to remove remaining ISI caused by the channel and the FF portion of the equalizer. A decision device produces a hard estimate of the transmitted symbol from a soft-decision estimate, obtained from the combined FF and FB filtering. All the constituent filters are assumed to be finite impulse response (FIR) filters.

B. MC–DFE: Analytical Framework

A mathematical framework of the MC–DFE is presented in [12] and [5]. The received signal is assumed to originate from a single source and to have already been preprocessed as described previously. Thus, the "received" signal is in discrete-time, complex-baseband form. A channel between the source and the ith sensor ($i = 1, 2, \ldots, N$) is modeled with a linear filter and additive noise. In such a model, the signal $u_i(n)$, received by a sensor i at discrete time n is

$$u_i(n) = \mathbf{g}_i^H(n)\mathbf{x}(n) + v(n) \tag{1}$$

where $\mathbf{g}_i(n)$ is a vector form of the ith channel impulse response at time n. The transmitted symbols that give rise to $u_i(n)$ are compactly represented with a column vector $\mathbf{x}(n)$.

Without loss of generality, all the channels are assumed to have the same length L_c. In addition, we assume the channels have the same lengths of the causal and anticausal parts, denoted, respectively, by L_c^c and L_c^a. Therefore, the vector $\mathbf{x}(n)$ is formatted as

$$\mathbf{x}(n) = [\, x(n + L_c^a) \quad \ldots \quad x(n) \quad \ldots \quad x(n - L_c^c + 1) \,]^T. \tag{2}$$

Similarly, the FF filters are assumed to have the same length L_{ff}. Also, their lengths of the causal and anticausal parts, denoted, respectively, by L_{ff}^c and L_{ff}^a, are equal.

The ith FF filter output at time n is driven by the received signals $u_i(n + L_{\text{ff}}^a), \ldots, u_i(n), u_i(n-1), \ldots, u_i(n - L_{\text{ff}}^c + 1)$. They are collected in a column vector $\tilde{\mathbf{u}}_i(n)$ which is expressed as

$$\tilde{\mathbf{u}}_i(n) = \mathbf{G}_i(n)\underline{\mathbf{x}}(n) + \mathbf{v}_i(n) \tag{3}$$

where $\mathbf{G}_i(n)$ is the L_{ff}-by-$(L_{\text{ff}} + L_c - 1)$ channel matrix, obtained by appropriately shifting and stacking $\mathbf{g}_i^H(n + L_{\text{ff}}^a), \ldots, \mathbf{g}_i^H(n - L_{\text{ff}}^c + 1)$ into its rows. The transmitted symbols $x(n + L_{\text{ff}}^a + L_c^a), \ldots, x(n - L_{\text{ff}}^c - L_c^c + 2)$ impacting $\tilde{\mathbf{u}}_i(n)$ are collected into a column vector $\underline{\mathbf{x}}(n)$. Similarly, $\mathbf{v}_i(n)$ is a compact vector representation of the noise samples influencing $\tilde{\mathbf{u}}_i(n)$.

Stacking up the vectors $\tilde{\mathbf{u}}_1(n), \tilde{\mathbf{u}}_2(n), \ldots, \tilde{\mathbf{u}}_N(n)$ into a column vector, a signal vector $\underline{\tilde{\mathbf{u}}}(n)$, which represents a signal received at the equalizer's FF section at time n, is constructed and given by

$$\underline{\tilde{\mathbf{u}}}(n) = \underline{\mathbf{G}}(n)\underline{\mathbf{x}}(n) + \underline{\mathbf{v}}(n) \tag{4}$$

where the noise vector $\underline{\mathbf{v}}(n)$ and (NL_{ff})-by-$(L_{\text{ff}} + N - 1)$ multichannel matrix $\underline{\mathbf{G}}(n)$ are constructed in a similar manner by stacking up the corresponding constituents vertically.

The input to the FB filter at time n is a sequence of the equalizer's estimates $\hat{x}(n-1), \ldots, \hat{x}(n - L_{\text{fb}})$, where L_{fb} is the FB filter length, which may be smaller than the channel length L_c. These estimates are collected in a column vector $\hat{\mathbf{x}}(n)$. Note that the index n corresponds to an index of a symbol that is being estimated.

A soft decision estimate $\hat{x}_{\text{soft}}(n)$ is evaluated as

$$\hat{x}_{\text{soft}}(n) = \mathbf{w}^H(n)\mathbf{u}(n) \tag{5}$$

where $\mathbf{w}(n) = [\,\mathbf{w}_1^T(n) \quad \dots \quad \mathbf{w}_N^T(n) \quad -\mathbf{w}_{\rm fb}^T(n)\,]^T$ is the equalizer's weight vector (i.e., its impulse response) and $\mathbf{u}(n) = [\,\underline{\tilde{\mathbf{u}}}^T(n) \quad \hat{\mathbf{x}}^T(n)\,]^T$ is the input to the equalizer at time n. A hard decision estimate $\hat{x}(n)$ is computed from $\hat{x}_{\rm soft}(n)$ and the constellation diagram of the signaling employed in the communication scheme.

As a final remark, note that the overall number of equalizer coefficients is

$$m = NL_{\rm ff} + L_{\rm fb}. \tag{6}$$

C. MC–DFE: Optimization of Weights

The equalizer weights $\mathbf{w}(n)$ are evaluated with respect to some optimization criterion. A minimization of the MSE between the transmitted symbol $x(n)$ and its soft decision estimate $\hat{x}_{\rm soft}(n)$ is one of the most popular approaches, in which the weight vector $\mathbf{w}(n)$ is chosen such that the signal prediction MSE

$$\xi(n) = \mathbf{E}\left[|x(n) - \hat{x}_{\rm soft}(n)|^2\right] \tag{7}$$

is minimized. The solution to this optimization problem is referred to as the MMSE receiver given by

$$\mathbf{w}_{\rm MMSE}(n) = \mathbf{R}^{-1}(n)\mathbf{r}(n) \tag{8}$$

where $\mathbf{R}(n)$ and $\mathbf{r}(n)$ are the ensemble correlation matrix of the input signal and cross-correlation vector between the input and desired output signal. They are evaluated as

$$\mathbf{R}(n) = \mathbf{E}\left[\mathbf{u}(n)\mathbf{u}^H(n)\right] \tag{9}$$

$$\mathbf{r}(n) = \mathbf{E}\left[\mathbf{u}(n)x^*(n)\right]. \tag{10}$$

The signal prediction MSE of the MMSE filter $\mathbf{w}_{\rm MMSE}$ is after substituting (8) into (7), given by

$$\sigma^2_{\rm MMSE}(n) = \mathbf{E}\left[|x(n)|^2\right] - \mathbf{r}^H(n)\mathbf{R}(n)^{-1}\mathbf{r}(n). \tag{11}$$

The ensemble statistics are rarely known and are replaced by time-average statistics. The cost function for an exponential weighting of the time-average statistics is [18]

$$C(n) = \sum_{i=1}^{n} \lambda^{n-i}|\mathbf{w}^H(n)\mathbf{u}(i) - x(i)|^2 \tag{12}$$

where $\lambda \leq 1$ is a positive forgetting factor which accommodates the time variability of the channel by reducing the impact of past data which is less relevant than current data for the current estimation problem.

A weight vector which minimizes this cost function is evaluated via

$$\mathbf{w}(n) = \hat{\mathbf{R}}^{-1}(n)\hat{\mathbf{r}}(n) \tag{13}$$

where $\hat{\mathbf{R}}(n)$ and $\hat{\mathbf{r}}(n)$ are the exponentially weighted sample correlation matrix (SCM) and input-desired output cross-correlation vector, given by

$$\hat{\mathbf{R}}(n) = \sum_{i=1}^{n} \lambda^{n-i}\mathbf{u}(i)\mathbf{u}^H(i) \tag{14}$$

$$\hat{\mathbf{r}}(n) = \sum_{i=1}^{n} \lambda^{n-i}\mathbf{u}(i)x^*(i). \tag{15}$$

The described method of updating equalizer coefficients is referred to as a direct adaptation approach and is of our interest in this paper. In comparison, the equalizer weights can also be calculated based upon the estimates of the channel impulse response for each sensor and the ensemble statistics of the observation noise. This approach is labeled as a channel-estimate-based equalization and is studied in [5].

III. Challenges in Multichannel Equalizer Design

The structure of the multichannel equalizer and the LS-based adaptation algorithm, described in Section II, have been known for a long time and extensively used in practice. However, little is known in how to choose the number of sensors, separation between them, and length of the constituent filters so that the equalization performance is optimized. These challenges are studied in this paper and motivated in this section.

A. Deficient Sample Support and Optimal Number of Equalizer Coefficients

If the number of observations n is sufficiently many times larger than the number of coefficients m, the SCM (14) is an accurate estimate of the input ensemble correlation matrix. However, when operating in the underwater acoustic environment, the time interval over which the statistics of the received signal can be assumed to be constant is finite and possibly short [2]. Therefore, since the adaptation of the equalizer filter coefficients is best performed using observations over intervals over which these statistics are constant (time invariant), the number of observations might not be sufficient to accurately estimate the ensemble correlation matrix. In this case, the performance of the resulting equalizer filters will be degraded.

To qualitatively study how deficient sample support impacts the estimation accuracy of the SCM, the eigenvalues of a matrix are chosen to conveniently visualize and intuitively infer if and how much the SCM departs from the corresponding ensemble correlation matrix. To start, assume that we receive n observation vectors of length m which are samples of a zero-mean process with a correlation matrix $\mathbf{R}$ equal to the identity matrix. The m eigenvalues of $\mathbf{R}$ all equal one. To simulate how the eigenvalues of the SCM corresponding to the received process behave, we perform the following numerical experiment [19]. A number of realizations of SCMs corresponding to a zero-mean process with identity correlation matrix are generated. Each SCM has order m and is evaluated from n different observation vectors of the considered process using (14) with $\lambda = 1$. The eigenvalues of each SCM are computed, all obtained eigenvalues are collected, and the normalized histogram, of area 1, is evaluated.

The plots of normalized histograms for $m = 10$ sensors and $n = 20$ and $n = 60$ observation vectors are, respectively, shown in Fig. 2(a) and (b). As can be observed, the eigenvalues of the SCM are spread around the ensemble (i.e., true) eigenvalue 1 (whose multiplicity is 10). This indicates that the SCM and ensemble correlation matrix differ. The amount of spread gives an intuitive indication of how much the SCM departs from the

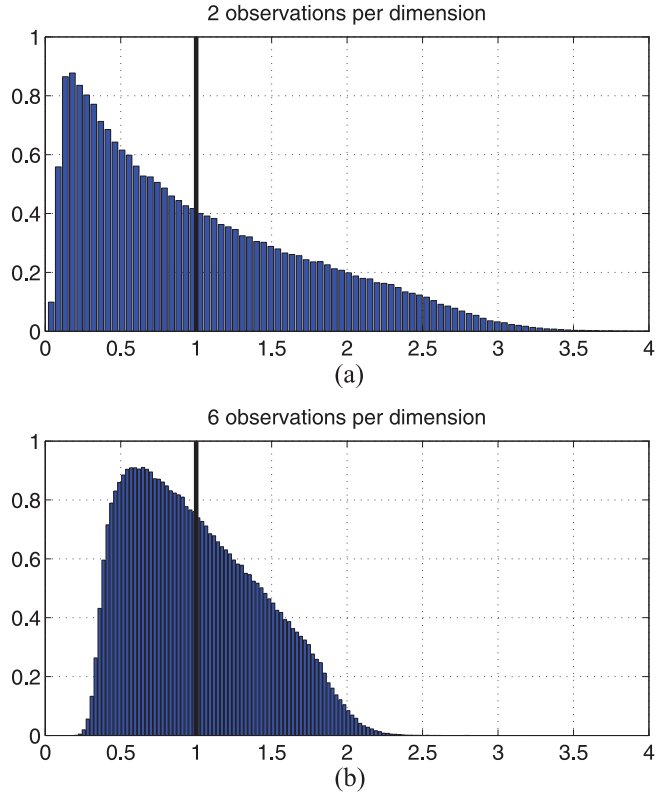

Fig. 2. Normalized histograms of the eigenvalues of sample correlation matrices corresponding to zero-mean process with a correlation matrix equal to the identity matrix, measured on $m = 10$ sensors. The number of observations n is 20 in (a) and 60 in (b). The ensemble eigenvalue is 1 and the underlying process is Gaussian distributed.

ensemble correlation matrix. Note that as the number of observations per dimension (n/m) increases from 2 [Fig. 2(a)] to 6 [Fig. 2(b)], the eigenvalues of the SCM concentrate around the ensemble eigenvalue.

The analytical characterization of how different functions of eigenvalues and eigenvectors of certain classes of random matrices behave is the main theme of random matrix theory (RMT). The SCM is a random matrix of our interest. Also, the histogram of the eigenvalues of an SCM is of particular interest because this function reveals insights in how the spread of sample eigenvalues around their ensemble counterparts depends on the number of observations per dimension.

One of the most famous RMT results is the Marčenko–Pastur law which analytically characterizes the normalized histogram of the eigenvalues corresponding to the SCM evaluated from the rectangularly windowed observations of a zero-mean process with identity correlation.[1] According to the law, in the limit when $m, n(m) \to \infty$ at the same rate such that $m/n \to c \in (0, \infty)$,[2] the normalized histogram is given by [21]

$$\mu(x) = \max\left(1 - \frac{1}{c}, 0\right)\delta_D(x) + \frac{\sqrt{(x-a)(b-x)}}{2\pi c x} I_{[a,b]}(x) \tag{16}$$

where $I_{[a,b]}(x) = 1$ for $a \leq x \leq b$ and is zero otherwise and $\delta_D(x)$ denotes the Dirac delta function. The support of (16) is compact with endpoints $a = (1 - \sqrt{c})^2$ and $b = (1 + \sqrt{c})^2$.[3]

The plots of Marčenko–Pastur law [see (16)] for different values of parameter c are shown in Fig. 3. Note that the ensemble eigenvalue of the considered process is 1 (of multiplicity m). It is intuitively clear that as c decreases, i.e., as more observations per dimension become available, the eigenvalues of the SCM concentrate around the ensemble eigenvalue. In other words, the SCM more accurately estimates the ensemble correlation matrix. The same reasoning applies when the input process is colored, i.e., the ensemble correlation matrix is not the scaled identity matrix. Again, the eigenvalues of the SCM are spread around their ensemble counterparts and as the number of observations per dimension $1/c$ increases, the sample eigenvalues concentrate around ensemble eigenvalues.

Due to channel time variability, the number of coefficients that can be adapted over the time interval within which the channel is approximately time invariant is limited such that a smaller number of coefficients might lead to better equalization performance. We present in Section IV the result which characterizes the signal prediction MSE of a multichannel DFE in time-varying channel, which has been derived using RMT in [22]. Using this result, we develop insights in how the number of sensors and lengths of the constituent filters impact the equalization performance.

B. Optimal Sensor Separation

Another challenge related to optimally configuring the multichannel equalizer is the selection of the separation between sensors. While the sensors in a MIMO system need to be sufficiently apart so that the signals at their outputs are uncorrelated [6], conventional wisdom is that array processing applications require that sensors be separated by no more than one half of the shortest wavelength of the received signals [7]. However, selection of optimal sensor separation is a more subtle problem because a vertical wave number spectrum of an inherently wideband signal impinging upon a vertical line array in an underwater acoustic communication channel has limited support (i.e., the received signal is sparse in a vertical wave number domain).

For experimental evidence that sensor separation is an important factor in determining equalizer performance, the following results obtained from processing the data collected in the Kauai Acomms Multidisciplinary university research initiative (KAM11) field experiment [23], conducted west of Kauau, HI, USA, in early September 2011, are useful. The underwater acoustic communication signal received at a vertical linear and uniformly spaced array is processed through a multichannel DFE equalizer with motion compensation and the transmitted symbols are detected. The equalizers with three and four channels (sensors) are considered. Each considered equalizer contains 36 taps per sensor filter and 36 taps in the

[1]More precisely, the Marčenko–Pastur law characterizes the limiting eigenvalue density function [20].

[2]The asymptotic regime could be viewed as a formalism which enables a closed-form solution for the normalized histogram. However, due to rapid convergence, the asymptotic result fairly accurately characterizes practical cases of finite m and n.

[3]As a remark, the Marčenko–Pastur law is not restricted to any particular probability distribution. Therefore, although the process used to generate Fig. 2 is Gaussian, similar plots are obtained for other probability distributions which satisfy formal conditions of the Marčenko–Pastur law. Possible differences that may arise for small m and n are due to different rates of convergence which depends on the underlying probability distribution.

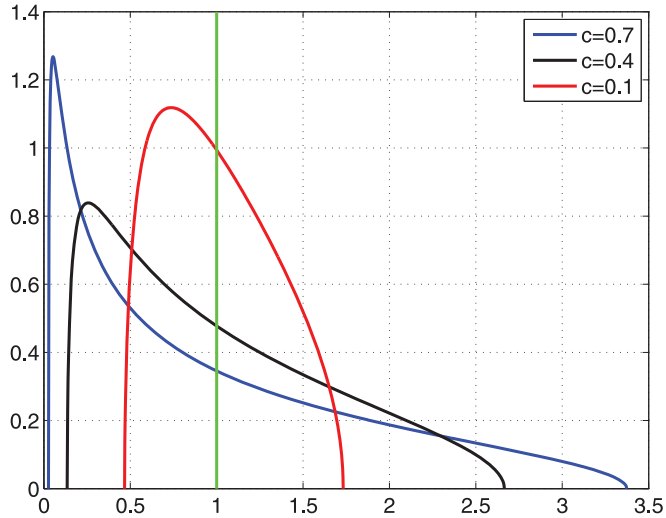

Fig. 3. Marčenko–Pastur law for different values of parameter c. The ensemble eigenvalue is 1 (its location is shown in green).

feedback filter. The fractional sampling rate is 2. The equalizer coefficients are adapted using the recursive least squares (RLS) algorithm using the forgetting factor λ which yields the best bit error rate (BER) performance. The measured BER versus sensor separation is shown in Fig. 4. The dotted and solid lines correspond to an experimental system whose consecutive hydrophones are, respectively, separated by 5 and 20 cm. As a remark, the minimal and maximal wavelengths corresponding to the signal of interest in the KAM11 experiment are, respectively, 9.03 and 17.06 cm.

IV. Performance Analysis of Equalization of Time-Varying Channels

The first part of this section presents the analytical characterization of the signal prediction MSE corresponding to the MC–DFE operating in time-varying channel. The second part discusses insights in how the number of equalizer coefficients impacts the equalization performance in time-varying channels. A numerical illustration of the presented insights concludes this section.

A. Signal Prediction MSE

The signal prediction MSE in the soft decision (i.e., the summed outputs of the FF and FB filters in Fig. 1) is adopted as the performance metric. To model the channel nonstationarity, we assume the channel is time invariant over a finite time interval and that the equalizer time-averaging window for the purpose of calculating equalizer filter coefficients is limited to this time interval length. These observations are processed by the MC–DFE equalizer which operates in a training mode. This means that the input to the FB filter are the true transmitted symbols as are the symbols $x(i)$ used in the calculation of $\hat{\mathbf{r}}(n)$ in (15). The analysis of training mode operation allows the analysis of the impact of channel time variability and thus limited observations intervals to be handled in a clearer manner and provides useful insights into performance tradeoffs. Other contributions to the performance analysis of equalizers also assume operation in the training mode [5], [16].

Intuitively, when infinitely many observations are used to train the equalizer weights, the LS-based MC–DFE with the rectangular window (i.e., a forgetting factor $\lambda = 1$) approaches the MMSE MC–DFE equalizer for a time-invariant channel. The impulse response vector $\mathbf{w}_{\mathrm{MMSE}}$ of the MMSE filter and the corresponding signal prediction MSE [also called the minimum achievable error (MAE)] σ^2_{MMSE}, given by (11), are conditioned on the impulse response of the transmission channel.

However, when the number of observations n used to adapt the equalizer weights is finite, the signal prediction MSE is larger than the minimum achievable error (MAE) and is given by [20], [22]

$$\mathbf{E}\left[|\xi(n)|^2\right] \approx \frac{n-1}{n-(NL_{\mathrm{ff}}+L_{\mathrm{fb}})-1}\sigma^2_{\mathrm{MMSE}} \qquad (17)$$

which is valid for $n > m+1$, where $m = NL_{\mathrm{ff}} + L_{\mathrm{fb}}$. The above result is derived in the Appendix and holds when 1) m and n grow to infinity at the same rate such that $m/n \to c \in (0,1)$; or 2) when the received signal is Gaussian, which happens if the transmitted signal is Gaussian itself, or the channel is long enough such that the received signal is Gaussian due to the central limit theorem. The asymptotic result holds for finite and relatively small m and n due to fast convergence rate inherent to random matrix theory results. While the performance prediction with (44) is more accurate for larger m and n, a reasonable accuracy (with error up to 1 dB) is obtained, for example, when binary symbols are transmitted through a short channel of length 4 or 5, while m and n are around 10.

The derived characterization reveals that the signal prediction MSE at the LS-based MC–DFE output is proportional to the signal prediction MSE at the MMSE equalizer output (i.e., the minimal achievable error σ^2_{MMSE}), and the proportionality constant does not depend on the channel impulse response. Note, however, that σ^2_{MMSE} does depend on the noise and channel characteristics as well as the lengths of the equalizer's feedforward and feedback filters.

B. Insights Into the Expression for Signal Prediction MSE

This part considers a problem of determining an optimal number of coefficients in a multichannel DFE equalizer which optimizes the signal prediction MSE. We assume the number of sensors (channels) of a multichannel equalizer is fixed and analyze how the number of coefficients contained in the equalizer's constituent filters impacts the signal prediction performance.

The insights into effects that impact the optimal number of coefficients which minimizes the signal prediction MSE could be gained from the characterization of the signal prediction MSE (44).

Namely, the constant of proportionality in (44) is an increasing function of the overall number of equalizer weights m when the number of observations n is fixed. On the other hand, the MAE σ^2_{MMSE} can be shown to be a monotonically nonincreasing function of the equalizer length m. Therefore, the signal prediction MSE is minimized at a point where these two competing effects are balanced.

In other words, the optimal equalizer is a tradeoff between the MMSE requirements and those justified by the RMT insights. From the point of view of minimizing the MAE, the fact that the

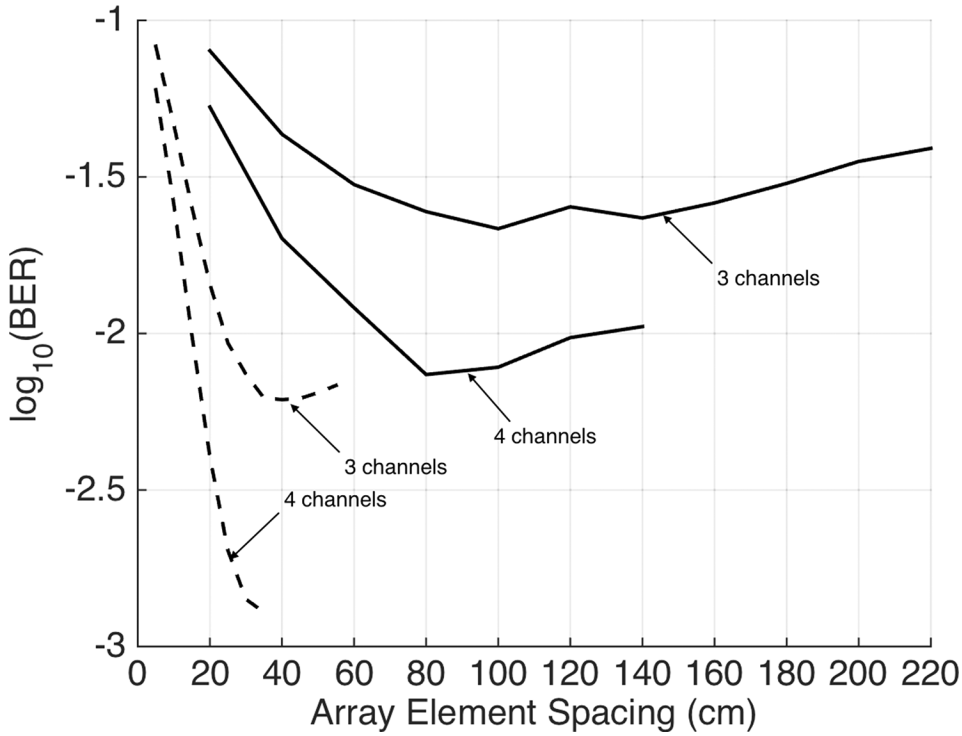

Fig. 4. Experimentally measured BER versus sensor separation for three- and four-sensor DFE equalizer with motion compensation, 36 taps per sensor filter, and 36 taps in a feedback filter. The solid and dashed lines correspond to two different experimental systems, as explained in Section III-B.

channel has a finite impulse response indicates that the best filter should be an infinite impulse response (IIR) filter. However, the best estimate of the sample correlation matrix $\hat{\mathbf{R}}(n)$ when the number of stationary observations n is fixed (and controlled by the channel) is achieved if the order of the SCM m is 1, i.e., if there is only one equalizer coefficient. The best balance will occur somewhere between these two extremes.

To illustrate how the number of stationary observations n impacts the quality of the SCM, we recall the Marčenko–Pastur law from Section III. As shown in Fig. 3, the spread of the eigenvalues of the SCM corresponding to observations of zero-mean process of identity correlation around the ensemble eigenvalue depends on parameter c, whose inverse represents the number of observations per degree of freedom. Thus, as the value of parameter c decreases, the eigenvalues of the SCM concentrate around the ensemble eigenvalue and hence, the SCM more accurately estimates the ensemble correlation matrix.

Another insightful characterization of the signal prediction MSE is obtained by representing it as a sum of the MAE and excess error such that

$$\mathbf{E}\left[|\xi(n)|^2\right] \approx \sigma^2_{\mathrm{MMSE}} + \frac{m}{n-m-1}\sigma^2_{\mathrm{MMSE}}. \qquad (18)$$

Note that the excess error is viewed as a product of the factor which depends only on the number of equalizer weights m and averaging interval n and the MAE σ^2_{MMSE}, which is a function of the channel impulse response and the number of coefficients m.

The conclusion that the optimal number of equalizer coefficients is a tradeoff between the MMSE requirements and those justified by the RMT insights is numerically illustrated in the following part.

C. Numerical Illustration

In the first example, we consider an LTI channel whose impulse response is shown in Fig. 5. The transmitted symbols are binary $\{+1, -1\}$ with uniform distribution. They are transmitted through the considered channel and noise is added to the obtained symbols. The Gaussian distributed noise is nonwhite and generated such that its correlation properties correspond to the ambient ocean noise [24]. The received signal is processed through a single-channel DFE equalizer. The signal prediction MSE corresponding to the MMSE equalizer coefficients is evaluated using (11). Its dependence on the number of taps contained in the FF and FB filters is shown in Fig. 6 for signal-to-noise ratio (SNR) of 0 dB [Fig. 6(a)] and SNR of 10 dB [Fig. 6(b)]. As expected, the signal prediction performance improves as the number of equalizer coefficients increases.

A tradeoff between the MMSE requirement for longer filters and random matrix theory insight which favors shorter equalizers is visualized by showing the dependence of the signal prediction MSE on the FF and FB filter lengths. This dependence is shown in Fig. 7 for the received SNR of 0 dB [Fig. 7(a)] and 10 dB [Fig. 7(b)]. We assume that the observation interval for the estimation of the signal statistics (n) is 150 symbols.

The number of coefficients in the constituent filters of the optimal DFE which minimizes the signal prediction MSE for different SNRs is shown in Table I. The channel impulse response is as shown in Fig. 5, and the averaging interval is 150. As shown in Table I, for a given, fixed averaging interval, the optimal number of coefficients increases with SNR. In addition, the optimal distribution of coefficients between the constituent filters with increasing SNR is such that the number of coefficients in the FF filter decreases, while the number of coefficients in the FB filter increases.

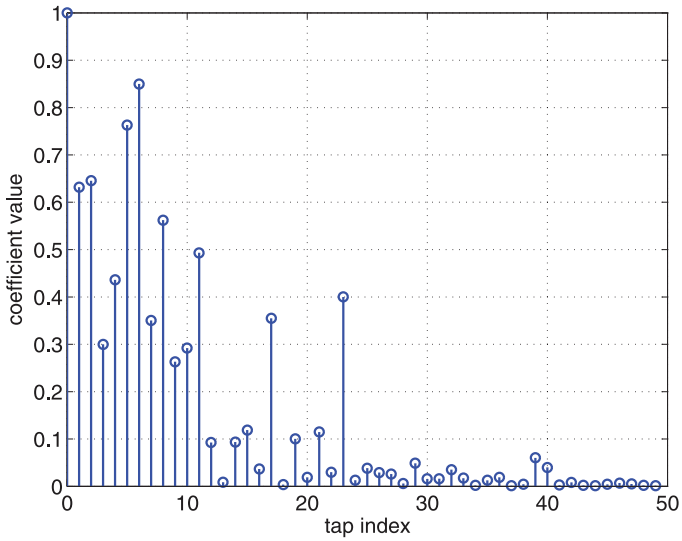

Fig. 5. Channel impulse response used in simulations.

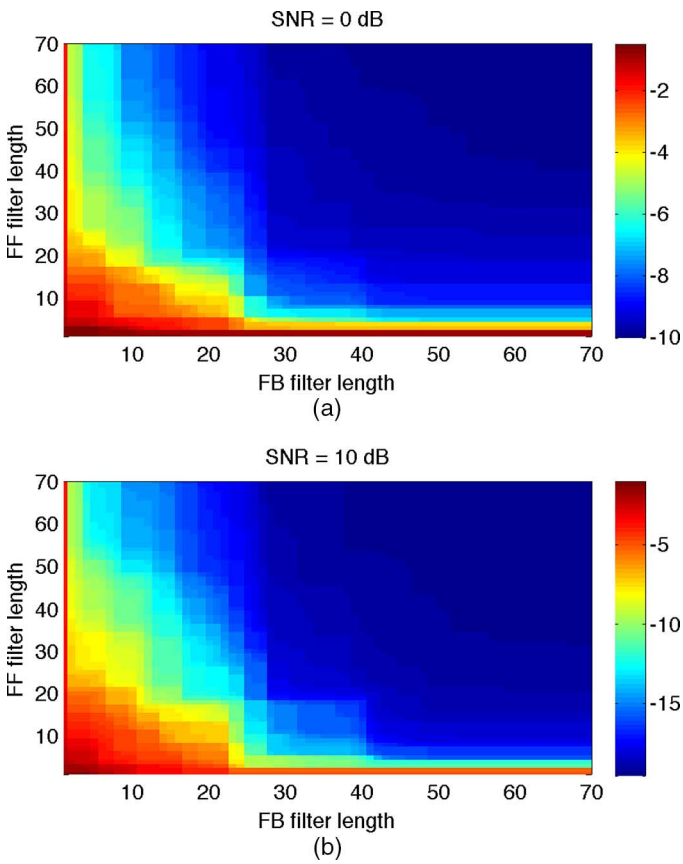

Fig. 6. Minimum achievable signal prediction MSE in decibels versus the number of taps in FF and FB filters of the DFE equalizer for (a) SNR $=$ 0 dB and (b) SNR $=$ 10 dB. The impulse response of the transmission channel is given in Fig. 5.

Intuitively, the FF filter is the only one that can attenuate noise. On the other hand, both filters attenuate ISI. However, the FF filter can only attenuate ISI to the extent that it has a different temporal signature than the desired symbol. Consequently, more coefficients are allocated to the FF filter at low SNR than at high SNR in order to reduce noise. On the other hand, when SNR gets large, ISI is the dominant source of distortion so that the optimal

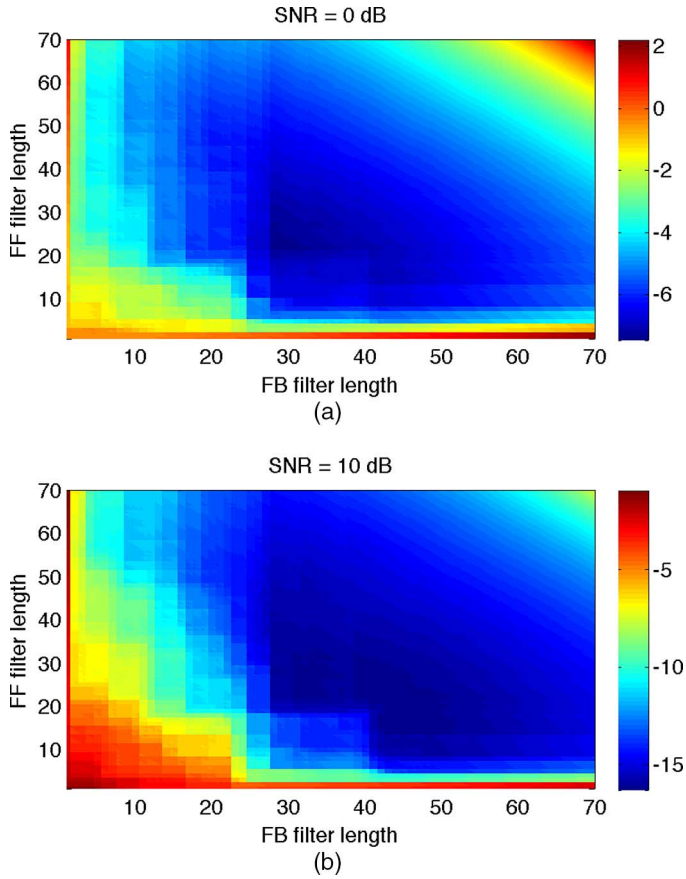

Fig. 7. Analytically computed signal prediction MSE in decibels versus the number of taps in FF and FB filters of the DFE equalizer for (a) SNR $=$ 0 dB and (b) SNR $=$ 10 dB. The impulse response of the transmission channel is given in Fig. 5. The number of snapshots (the $\approx$ number of received symbols) is 150.

TABLE I
OPTIMAL NUMBER OF COEFFICIENTS

SNR	0 dB	5 dB	10 dB	12 dB	14 dB	15 dB	20 dB	25 dB
L_{ff}	22	22	22	16	15	15	15	15
L_{fb}	28	31	41	48	48	48	48	48
m	50	53	63	64	63	63	63	63

number of coefficients in the FB filter increases in order to eliminate ISI.

In the second example, we consider the optimal MC–DFE design for the underwater acoustic communication channel observed during the KAM11 field experiment [23]. The number of channels (sensors) is 5, and a snapshot of a channel impulse response between a source and one of the sensors is shown in Fig. 8. The dependence of the signal prediction MSE on the lengths of FF and FB filters for received SNR of 22 dB and experimentally observed spatially correlated ambient noise is shown in Fig. 9. The observation interval for the adaptation of filter weights is 500 symbols. It can be noted that the optimal equalizer uses 16 taps in each FF filter and 10 taps in an FB filter and achieves signal prediction MSE of -7.33 dB.

In comparison to a single channel equalizer considered in the previous example, the optimal number of FF filter taps in a multichannel equalizer is larger than the number of FB filter taps

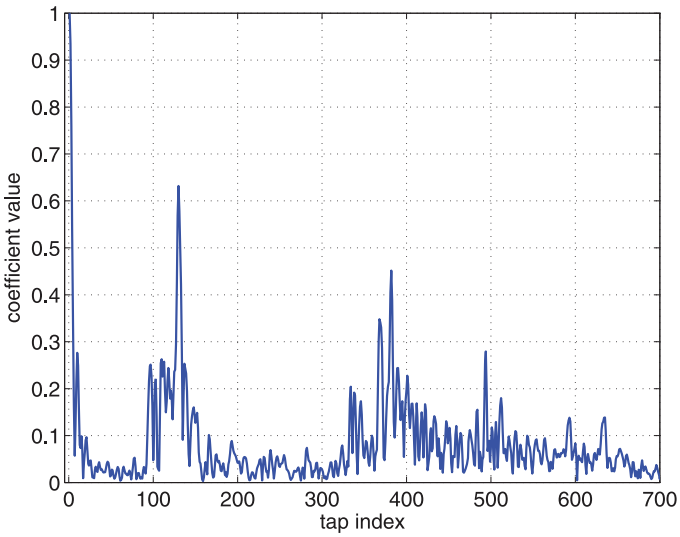

Fig. 8. Channel impulse response at one of the sensors during the KAM11 experiment.

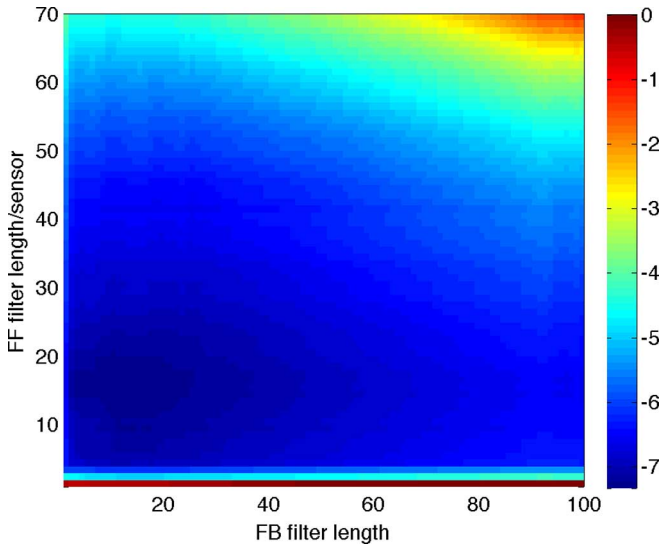

Fig. 9. Signal prediction MSE in decibels versus the number of taps in the FF filter per sensor and the number of taps in the FB filter. The number of sensors is 5, and channel impulse response and spatially correlated ambient noise are as observed in the field experiment. The received SNR is 22 dB, and the channel coherence time is 500 symbols.

at (high) SNR of 22 dB. Intuitively, this is because multiple channels in a multichannel equalizer are utilized for spatial processing to attenuate noise and eliminate ISI because different arrivals come from slightly different directions. Therefore, even at high SNR when ISI is the dominant source of distortion, sensor filters have better ability to reduce ISI through combining the spatial and delay domain processing.

The ability of the multichannel equalizer to eliminate ISI as well as attenuate noise is dependent on the number and spacing of the sensors in the array (and thus the total aperture as well). The analysis of this dependence is addressed in Section V.

V. Sparse Wideband Channel

This section develops a theoretical framework suitable for analyzing and gaining insights into how the equalizer performance depends on the array design, i.e., the selection of the number of and separation between the sensors. We first present the arrival

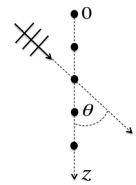

Fig. 10. Pictorial illustration of the coordinate system associated with the array of sensors. Note that the topmost sensor is located at the origin and the z-axis is oriented downward.

model consisting of a finite number of wideband and spatially spread arrivals impinging on an array of sensors. The input correlation matrix and cross-correlation vector are then evaluated for the described arrival model.

Without loss of generality, this section considers linear multichannel equalization. However, the model could be extended to include a multichannel DFE.

A. Arrival Model

We assume that a single source is isotropically transmitting a wideband signal of power 1, confined within a frequency range between ω_L and ω_U rad/s. The one-sided power spectrum density of the transmitted signal is given by[4]

$$P_x(\omega) = \begin{cases} P_0, & \text{if } \omega \in [\omega_L, \omega_U] \\ 0, & \text{otherwise.} \end{cases} \tag{19}$$

We assume that on the receiver side, a linear vertical and uniformly spaced array of sensors with sensor separation d is receiving the transmitted signal. The coordinate system has the origin at the position of the top-most sensor and its z-axis is along the array and oriented downward, as shown in Fig. 10. The projection of the spatial wave number vector $\mathbf{k}$ onto the z-axis is denoted with k_z. The directional cosine is defined as $u = \cos(\theta)$, where θ is the elevation angle with respect to the array such that $\theta = 90^\circ$ corresponds to the arrival from the broadside of the array, while $\theta = 0^\circ$ corresponds to the arrival propagating down the array.

To model the received signal, we assume that the underwater acoustic communication system is wideband as is the case for most single carrier systems. Also, the impulse response of the underwater acoustic communication channel is sparse in the vertical wave number domain. Furthermore, processing of data from a variety of underwater acoustic communication experiments shows that the acoustic energy is usually confined to a limited region of the delay-vertical wave number domain. As an example, the distribution of acoustic energy, received in the field experiment (KAM11) [23], across the elevation angle and delay domains, averaged over the time period of 60 s, is shown in Fig. 11.

Therefore, without loss of generality, we assume that the array receives acoustic energy from N_d different directions. The acoustic energy corresponding to each arrival is wideband and spatially spread in the angle domain.

To formalize the model, the transmission channel is viewed as a filter whose response in the $\omega - k_z$ domain has N_d nonzero,

[4]The power amplifier is part of the communication channel in this model. Hence, the signal at the input of a power amplifier is the transmitted signal in our model.

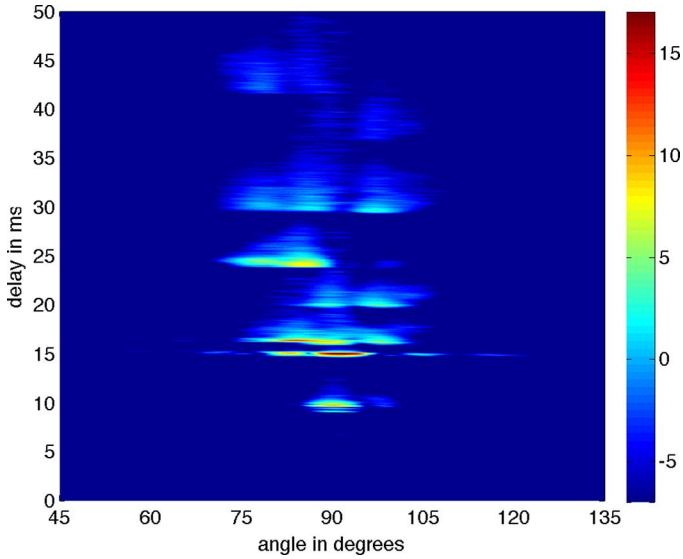

Fig. 11. Distribution of acoustic energy received in the field experiment, averaged over the time period of 60 s. The z-axis is in the decibel scale. The energy outside the region of elevation angles from 45° to 135° is below −7 dB.

nonoverlapping patches. Each patch gives rise to one arrival in the $\omega - k_z$ domain.[5] We assume the arrivals come from nonoverlapping ranges $[u_n^{(l)}, u_n^{(u)}]$, $n = 1, \ldots, N_d$, in the directional cosine domain. The channel response is thus given by[6]

$$H(\omega, k_z) = \sum_{n=1}^{N_d} h_n(\omega, k_z) \tag{20}$$

where the frequency response of a patch is given by

$$h_n(\omega, k_z) = \begin{cases} |h_n| e^{-j\omega\tau_n(k_z)}, & \omega \in [\omega_L, \omega_U] \text{ and} \\ & k_z(\omega) \in \left[\frac{\omega}{c}u_n^{(l)}, \frac{\omega}{c}u_n^{(u)}\right] \\ 0, & \text{otherwise} \end{cases} \tag{21}$$

where $\left[(\omega/c)u_n^{(l)}, (\omega/c)u_n^{(u)}\right]$, $n = 1, \ldots, N_d$, are disjoint segments and $\tau_n(k_z)$ models a relative delay within and between arrivals. Here we assume that the delay within each patch is much smaller than the relative delay between patches such that $\tau_n(k_z) \approx \tau_n$.

Given the channel model, the frequency/wave number spectrum of the received signal $P_y(\omega, k_z)$ is then given by

$$P_y(\omega, k_z) = |H(\omega, k_z)|^2 P_x(\omega). \tag{22}$$

The presented arrival model can be extended to mimic more realistic cases which include nonflat frequency responses over the possibly overlapping patches in the frequency/wave number domain, as well as a more general shape of an array of sensors. However, for the purpose of gaining insights in how sensor separation impacts the performance, the more important aspect of the model is that it accounts for wideband and spatially spread nature of the received signal.

In the following parts, we evaluate the correlation matrix and cross-correlation vector corresponding to the considered model.

[5]Note that in our terminology, an "arrival" is a patch of energy in a frequency/wave number domain rather than a single impulse in a delay domain, as is commonly interpreted.

[6]We assume that the power amplification is absorbed in the channel response.

B. Evaluation of Correlation Matrix

The ensemble correlation matrix $\mathbf{R}$ is obtained from the space–time correlation function $\rho_{uu^*}(\tau, \Delta\mathbf{p})$ of the received signal, defined as

$$\rho_{uu^*}(\tau, \Delta\mathbf{p}) = \mathbf{E}\left[u(t, \mathbf{p})u^*(t - \tau, \mathbf{p} - \Delta\mathbf{p})\right] \tag{23}$$

where $u(t, \mathbf{p})$ is the continuous signal received at time t and position $\mathbf{p}$ in the associated coordinate system. The sample of the continuous time signal $u(t, \mathbf{p})$ received at sensor i at discrete time n is denoted by $u_i(n)$. In general, the space–time correlation function describes the correlation between the signals received at points spatially separated by vector $\Delta\mathbf{p}$ and at time instances separated by a delay τ. However, we are only interested in correlation between signals received by sensors in an array. Since the sensors are aligned along the z-axis, the second argument in the space–time correlation function (23) is $\Delta\mathbf{p} = \mathbf{i}_z\Delta p$, where Δp is the separation between sensors and $\mathbf{i}_z$ is the unit vector along the z-axis. The correlation function $\rho_{uu^*}(\tau, \mathbf{i}_z\Delta p)$ is evaluated from the frequency/wave number spectrum of the received signal and is given by[7] [7]

$$\begin{aligned} &\rho_{uu^*}(\tau, \mathbf{i}_z\Delta p) \\ &\quad = \frac{1}{(2\pi)^2}\int_{\omega_L}^{\omega_U}\int_{-\omega/c}^{+\omega/c} P_y(\omega, k_z)e^{-j(\omega\tau - k_z\Delta p)}dk_z d\omega \\ &\quad = \frac{1}{2\pi}\int_{\omega_L}^{\omega_U} S_y(\omega, \Delta p)e^{-j\omega\tau}d\omega \end{aligned} \tag{24}$$

where $S_y(\omega, \Delta p)$ is the temporal spectrum spatial correlation function.

The temporal spectrum spatial correlation function is for a considered channel response evaluated in a closed form

$$\begin{aligned} S_y(\omega, \Delta p) &= \frac{1}{2\pi}\int_{-\omega/c}^{+\omega/c} P_y(\omega, k_z)e^{jk_z\Delta p}dk_z \\ &= \frac{P_0}{\pi}\sum_{n=1}^{N_d} |h_n|^2 \Delta k_{z,n} e^{-j\bar{k}_{z,n}\Delta p}\mathrm{sinc}(\Delta k_{z,n}\Delta p) \end{aligned} \tag{25}$$

where $\mathrm{sinc}(x) = \sin(x)/x$ and

$$\bar{k}_{z,n} = \frac{\omega}{c}\frac{u_n^{(l)} + u_n^{(u)}}{2}, \quad \Delta k_{z,n} = \frac{\omega}{c}\frac{|u_n^{(u)} - u_n^{(l)}|}{2} \tag{26}$$

are the wave numbers corresponding to, respectively, the mean and width of the range of directional cosines pertaining to each arriving patch.

The space–time correlation function $\rho_{uu^*}(\tau, \mathbf{i}_z\Delta p)$ is then obtained by substituting (25) into (24) and carrying out the integration. The final result cannot be evaluated in a closed form for a given model and is computed numerically.

To specify the correlation matrix $\mathbf{R}$, we first note, from the construction of the signal vector $\mathbf{u}$ and definition (9), that the correlation matrix $\mathbf{R}$ is a block matrix whose block in the position (i, j) is

$$\tilde{\mathbf{R}}_{ij} = \mathbf{E}\left[\tilde{\mathbf{u}}_i\tilde{\mathbf{u}}_j^H\right] \tag{27}$$

[7]Note that when $\Delta\mathbf{p}$ along the z-axis, $\mathbf{k}\Delta\mathbf{p} = k_z\Delta p$.

where $i, j = 1, \ldots, m$. Recalling that the observation vector $\tilde{\mathbf{u}}_i$ collects all the samples of the received signal at sensor i, which impact the output of the associated filter at a particular instant, the element in the position (t, s) of $\tilde{\mathbf{R}}_{ij}$ is given by

$$\left[\tilde{\mathbf{R}}_{ij}\right]_{t,s} = \rho\left((t-s)T_s, \mathbf{i}_z(i-j)d\right) \tag{28}$$

where d is the sensor separation (i.e., the sampling interval in spatial domain) and T_s is the sampling interval in time domain.

C. Evaluation of Cross-Correlation Vector

The cross-correlation vector $\mathbf{r}$ is obtained from the cross-correlation function $\rho_{ux^*}(\tau, \mathbf{p})$, defined as

$$\rho_{ux^*}(\tau, \mathbf{p}) = \mathbf{E}\left[u(t, \mathbf{p})x^*(t-\tau)\right] \tag{29}$$

where $\mathbf{p}$ is the position vector in the associated coordinate system. Since we are interested in evaluating the statistics of the signals received on the array, $\mathbf{p} = \mathbf{i}_z p$, where p is a (scalar) distance between the origin and a particular sensor and $\mathbf{i}_z$ is the unit vector along the z-axis. Recall that the cross-correlation function between the input and the output from a linear time-invariant filter is given as the inverse Fourier transform of the cross-spectral density. The cross-spectral density is evaluated as a product of the channel frequency response and power spectral density of the input process [25]. Analogously, the cross-correlation function $\rho_{ux^*}(\tau, \mathbf{i}_z p)$ is evaluated as[8]

$$\rho_{ux^*}(\tau, \mathbf{i}_z p) = \frac{1}{(2\pi)^2}\int_{\omega_L}^{\omega_U}\int_{-\omega/c}^{\omega/c} P_x(\omega)H(\omega, k_z)e^{j(\omega\tau - k_z p)}dk_z d\omega. \tag{30}$$

Denoting with $\tilde{S}_{ux^*}(\omega, p)$ the solution to the integration in (30) over k_z, the cross-correlation function is expressed as

$$\rho_{ux^*}(\tau, \mathbf{i}_z p) = \frac{1}{2\pi}\int_{\omega_L}^{\omega_U} \tilde{S}_{ux^*}(\omega, p)e^{-j\omega\tau}d\omega. \tag{31}$$

The function $\tilde{S}_{ux^*}(\omega, p)$ is for the considered model evaluated in a closed form and given by

$$\begin{aligned}\tilde{S}_{ux^*}(\omega, p) &= \frac{1}{2\pi}\int_{-\omega/c}^{+\omega/c} P_x(\omega, k_z)H(\omega, k_z)e^{-jk_z p}dk_z \\ &= \frac{P_0}{\pi}\sum_{n=1}^{N} h_n \Delta k_{z,n} e^{-j\bar{k}_{z,n}p}\mathrm{sinc}(\Delta k_{z,n} p)\end{aligned} \tag{32}$$

where $\Delta k_{z,n}$ and $\bar{k}_{z,n}$ are as defined in (26).

The cross-correlation function $\rho_{ux^*}(\tau, \mathbf{i}_z p)$ is finally obtained by substituting (32) into (31) and carrying out the integration. The final result is computed numerically.

To specify the cross-correlation vector $\mathbf{r}$, we first note that it has a block structure whose lth block $\tilde{\mathbf{r}}_l$ is the cross-correlation vector between the observation vector $\tilde{\mathbf{u}}_l$ and the transmitted signal x. Since $\tilde{\mathbf{u}}_l$ collects the time samples of the signal received at sensor l which impact the output of the associated filter at a particular instant, the sth element in $\tilde{\mathbf{r}}_l$ is thus given by

$$\left[\tilde{\mathbf{r}}_l\right]_s = \rho_{ux^*}\left(sT_s, \mathbf{i}_z l d\right) \tag{33}$$

[8]Note that vector $\mathbf{p}$ is aligned along the z-axis because we are interested in the statistics of the signal received on the array of sensors. Thus, $\mathbf{k}\mathbf{p} = k_z p$.

where d and T_s are the sampling intervals in, respectively, spacial and delay domains.

VI. Equalizer Design: Optimal Array Selection

This section illustrates how the number of sensors and their separation impact the signal prediction performance of the MMSE and LS adapted multichannel equalizer for a particular arrival structure.

The dependence of signal prediction MSE on the number of sensors and their separation is examined by using (11) and (44) for a particular arrival structure. The theoretical framework presented in Section V is used to evaluate the correlation matrix $\mathbf{R}$ and cross-correlation vector $\mathbf{r}$ corresponding to the considered arrival structure.

A. Optimal Sensor Separation

To illustrate that the equalization performance is optimized for a finite sensor separation which is not necessarily equal to one half of the shortest wavelength, we consider a particular arrival model whose bandwidth is between 9 and 17 kHz, motivated by the KAM11 experiment [23]. For a sound speed of 1535 m/s, as observed in some of the KAM11 data epochs, the corresponding wavelengths are between 9.03 and 17.06 cm.

Here we consider an arrival model for which the acoustic energy arrives from the ranges of elevation angles of [89°, 91°] and [84°, 86°]. The corresponding channel responses are equal, i.e., $|h_1| = |h_2|$, and the relative delay between the arrivals is much larger than the delay within each patch and is equal to two sampling periods, i.e., $\tau_2 - \tau_1 = 2/F_s$, where $F_s = 40$ kHz is the sampling frequency. Note that for a given signal bandwidth of 8 kHz, the arrivals are not resolvable in the delay domain. The ambient noise is directional and has power 1. It is confined within the range of elevation angles between 80° and 100°. The SNR is 10 dB. The linear multichannel equalizer contains ten sensors. The parameters of the communication system and the arrival model are summarized in Table II.

The dependence of the signal prediction MSE on sensor separation when the statistics of the input process are known such that the equalizer coefficients are evaluated using (8) and the equalizer has one tap in each sensor filter is shown in Fig. 12. The case when each sensor filter contains five taps is shown in Fig. 13. As can be observed, the performance is optimized for a finite sensor separation which is greater than one half of the shortest wavelength of the signals of interest.

When the statistics of the input process are unknown and estimated from the received data, the signal prediction MSE is proportional to the signal prediction MSE corresponding to the MMSE processor, as given by (44). Hence, the dependence of the signal prediction MSE on sensor separation for the considered arrival model and multichannel equalizer is as shown in Figs. 12 and 13 up to an appropriate scaling of the vertical axes. The scaling depends on the averaging window size and an overall number of coefficients.

Finally, as an illustration, the dependence of signal prediction MSE on the number of sensors and their separation when the equalizer weights are computed using the LS solution (13) and the channel is nonstationary and approximately time invariant over 500 symbols is shown in Fig. 14. The signal prediction

TABLE II
EXAMINED SYSTEM AND ARRIVAL MODEL

Bandwidth	9 kHz − 17 kHz
Sampling Frequency	$F_s = 40$ kHz
Sound Speed	1535 m/s
Wavelengths	9.03 − 17.06 cm
Arrival 1	$[89^o, 91^o]$, $\lvert h_1\rvert$, τ_1
Arrival 2	$[84^o, 86^o]$, $\lvert h_2\rvert = \lvert h_1\rvert$, $\tau_2 - \tau_1 = 2/F_s$
Noise in angular domain	$[80^o, 100^o]$
SNR	10 dB
Number of sensors	10

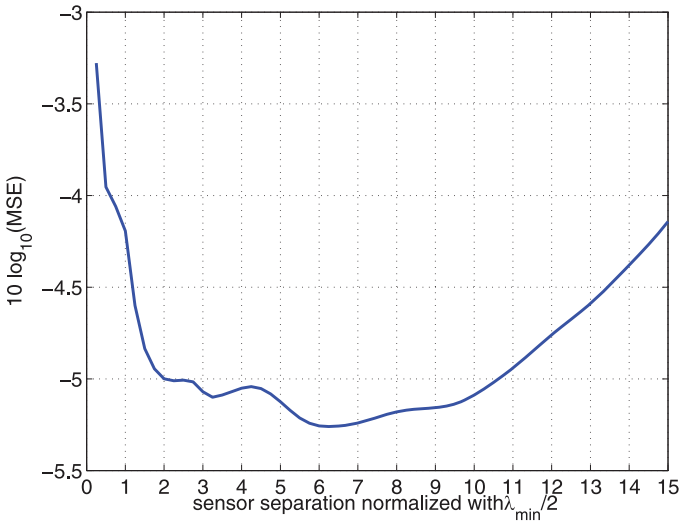

Fig. 12. Signal prediction MSE versus sensor separation for the MMSE linear equalizer. The sensor separation in normalized with the half-a-wavelength corresponding to the highest frequency of interest. Each of the ten single sensor feedfoward filters has a length of one tap.

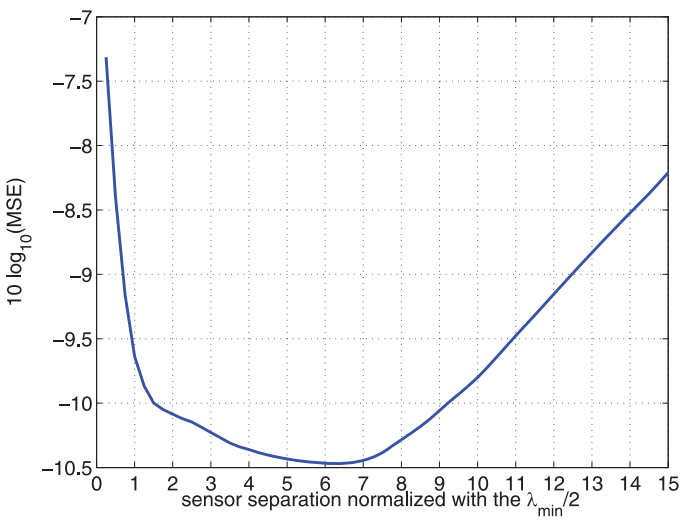

Fig. 13. Signal prediction MSE versus sensor separation for the MMSE linear equalizer. The sensor separation in normalized with the half-a-wavelength corresponding to the highest frequency of interest. Each of the ten single sensor feedfoward filters has a length of five taps.

MSE is evaluated using (44). Under the constraint that each sensor filter has five taps, the signal prediction performance is

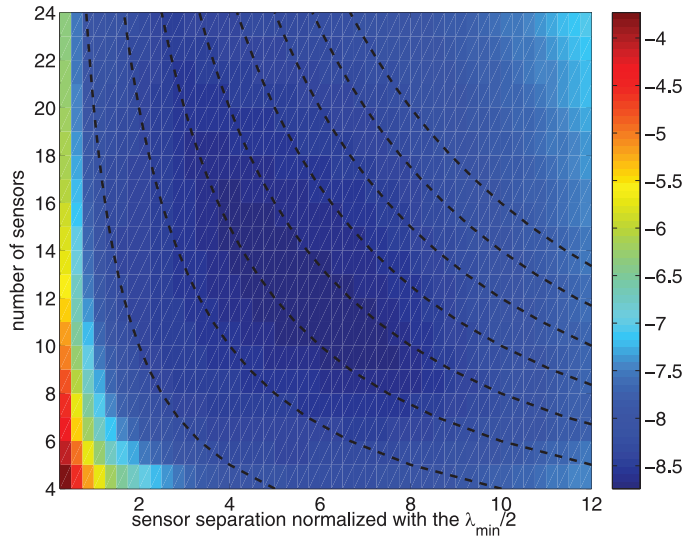

Fig. 14. Signal prediction MSE versus the number of sensors and sensor separation for the LS-based linear equalizer. The sensor separation in normalized with the half-a-wavelength corresponding to the highest frequency of interest. The dashed lines are curves of constant aperture.

optimized when the equalizer contains 12 sensors and their separation is almost $6\lambda_{\min}/2$, where $\lambda_{\min} = 9.03$ cm. Note the lines of constant aperture shown in Fig. 14. This effect is examined in Sections VI-B and VI-C.

B. Insights Into Optimal Sensor Separation

The insights in why the equalization performance depends on sensor separation as described in Section VI-A are presented in this section.

First, recall that increasing the separation between sensors in a vertical line array and keeping the number of sensors unchanged, the total array aperture increases, which in turn improves the resolution of the spatial filter [7]. On the other hand, if the sensors are separated by more than one half of the shortest wavelength of the signal of interest, the signal is spatially undersampled, which in turn causes the appearance of the grading lobes in the array beampattern [7].

The spatial degrees of freedom in a multichannel equalizer are exploited to coherently combine energy from different directions and to suppress ISI and noise. The optimal sensor separation depends on the arrival model and is a tradeoff between two competing requirements. On the one hand, increasing the sensor separation improves the resolution of the spatial filter which extracts the useful signal. On the other hand, those same degrees of freedom are getting squeezed into a smaller angular interval as the sensor separation increases. At some point, when the sensor separation is above a certain threshold, we lose ability to independently control the spatial filter response in the areas of the primary lobe and the grating lobes. Thus, when both primary and grating lobes fall in areas where signal is present, the spatial filter cannot independently control the response to get optimal signal combining or attenuation throughout the spatial interval containing the signal.

We use the example considered in Section VI-A and summarized in Table II to illustrate this tradeoff. To guide our thinking, beampatterns of the conventional beamformer corresponding

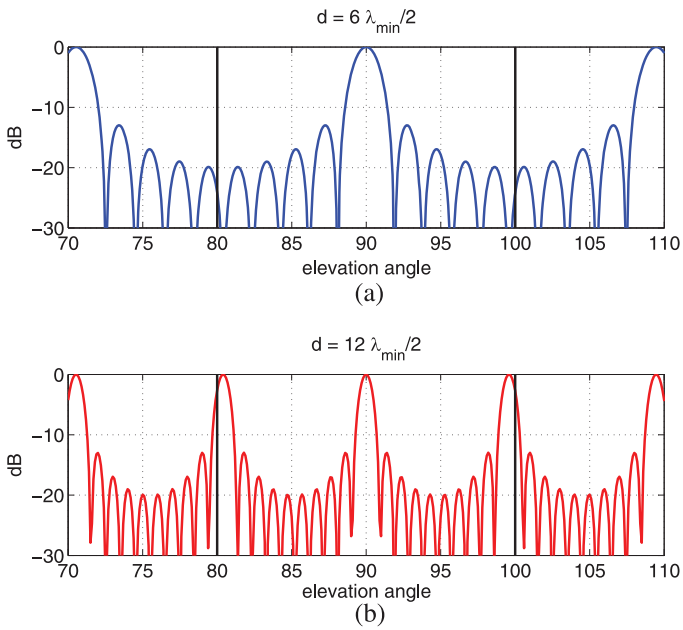

Fig. 15. Beampatterns of the ten-sensor conventional beamformer steered to the broadside for element separation of (a) $6\lambda_{\min}/2$ and (b) $12\lambda_{\min}/2$.

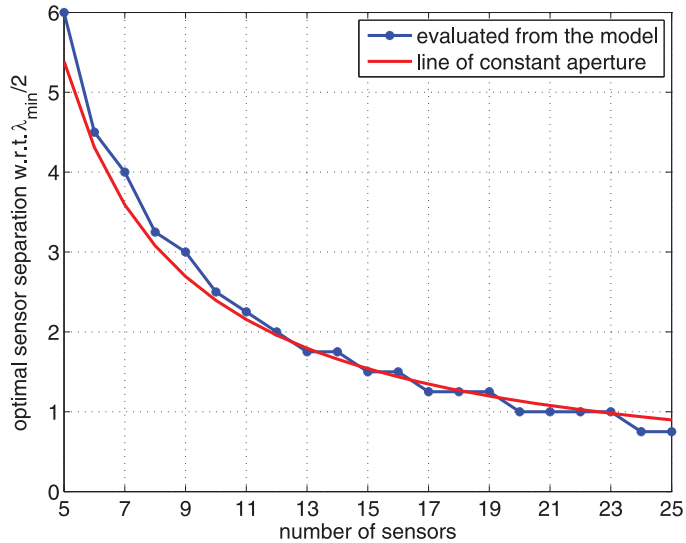

Fig. 16. Optimal sensor separation versus the number of sensors. Each sensor feedforward filter has seven taps. Each point on the blue curve optimizes the signal prediction MSE in the theoretical model. The red curve is the line of constant aperture, obtained from averaging the apertures corresponding to each point on the blue curve.

to a ten-sensor vertical line array with sensor separations of $6\lambda_{\min}/2$ and $12\lambda_{\min}/2$ are shown in Fig. 15(a) and (b), respectively.

Note that when the sensor separation is $6\lambda_{\min}/2$, the grating lobes fall outside the angular interval containing the signal (80° to 100°). As the spacing is increased beyond $6\lambda_{\min}/2$, the grating lobes begin to fall within the signal region until at a spacing of $12\lambda_{\min}/2$ the main lobe of the grating pattern falls within this region. Thus, as sensor separation increases beyond $6\lambda_{\min}/2$, the equalizer loses its ability to independently achieve the optimal gain for signals arriving from different angles of arrival in the signal region, and performance begins to degrade. Consequently, equalization performance is optimized for the sensor separation of $d_{\text{opt}} \approx 6\lambda_{\min}/2$, as can be confirmed from Figs. 12 and 13.

Thus, a rule of thumb is to increase sensor spacing up to the point where the grating lobes begin to impinge on the angular region of arriving signals or noise so as to maximize array resolution without sacrificing adaptability.

C. Optimal Array Aperture

The dependence of optimal sensor separation on the number of sensors and the number of taps per the sensor filter is illustrated here using the same arrival model as considered in Section VI-A. The only distinction is that the relative delay between two arrivals is $\tau_0 = 5/F_s$ so that longer sensor filters are needed to suppress the interference in the delay domain. Note that the arrivals are not resolvable in the delay domain.

The dependence of optimal sensor separation, normalized with one half of the shortest wavelength of the received signal, on the number of sensors when each sensor filter contains $L = 7$ taps is shown in Fig. 16. The statistics of the input signal are assumed known, and the optimal sensor separation optimizes (11). The input correlation matrix $\mathbf{R}$ and cross-correlation vector $\mathbf{r}$ for the considered model are evaluated as described in Section V.

As shown in Fig. 16, the optimal sensor separation decreases as the number of sensors increases in such a way that the array aperture is approximately constant. This is confirmed by plotting the constant aperture curve in Fig. 16, where the constant aperture is obtained from averaging the optimal apertures evaluated for the considered numbers of sensors.

The dependence of optimal sensor separation on the number of sensors N in the MMSE processor is for relatively shorter and relatively longer sensor filter lengths L shown in Fig. 17(a) and (b), respectively. As can be observed, the optimal array aperture is approximately constant and independent of L when $L \geq 7$. Recall that the relative delay between the arrivals in the considered example is $5/F_s$ and the taps in a sensor filter are separated by $1/F_s$. Therefore, the sensor filters containing $L \geq 7$ taps extend over both arrivals in the delay domain, and the processor suppresses the interference reasonably well.

On the other hand, when $L \leq 6$, the optimal sensor separation tends to increase as the length of sensor filters L decreases. In other words, given that the suppression capability is fairly limited in the delay domain due to short sensor filters, the aperture of the optimal processor increases so that the interference is better suppressed in the spatial domain. In addition, note that when the number of sensors N is not unreasonably small (i.e., N is above 4 in this example), the optimal aperture remains approximately constant.

The behavior of optimal aperture remains the same when equalizer coefficients are evaluated using the LS algorithm. Namely, recall that the signal prediction MSE of the LS-based equalizer is proportional to the signal prediction MSE corresponding to the MMSE processor. The constant of proportionality is a function of the number of coefficients and observation window length. Therefore, the optimal sensor separation which minimizes the signal prediction MSE for a given number of

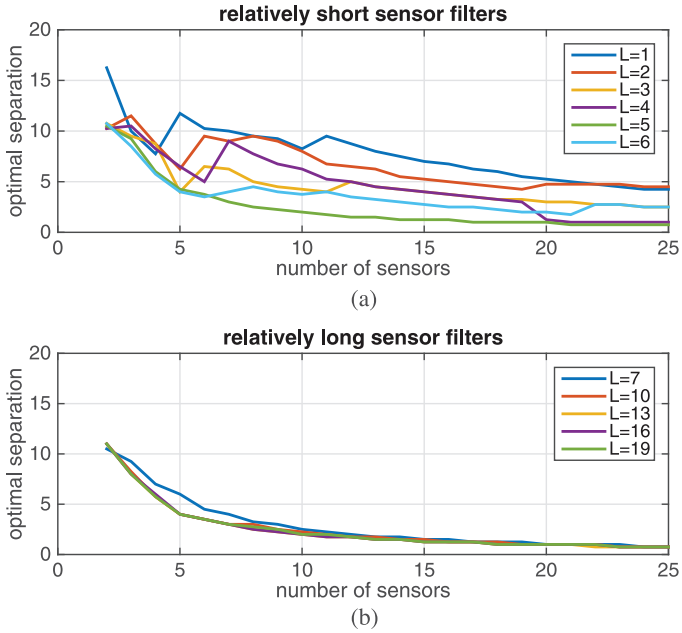

Fig. 17. Optimal sensor separation with respect to $\lambda_{\min}/2$ versus the number of sensors for (a) relatively shorter sensor filter lengths and (b) relatively longer sensor filter lengths.

sensors N and a number of taps per sensor filter L is the same for the MMSE and LS-based processors.

VII. Conclusion

The performance analysis and optimal design of multichannel equalizers of time-varying channels is presented in this paper. In the first part, an analytical characterization of the signal prediction MSE achieved at the output of the multichannel DFE equalizer operating in a nonstationary channel is presented. The channel is modeled as a frequency-selective filter which is time invariant over short time intervals such that the number of stationary observations used to adapt the equalizer weights is finite and limited. Further, the paper studies the problem of optimal selection of the number of equalizer coefficients. Namely, the obtained characterization of the equalization performance highlights that the optimal number of equalizer coefficients is a tradeoff between the MMSE requirement for longer filters and the insight that the finite number of observations can effectively adapt only a limited number of equalizer weights. This is validated via simulations and processing of experimentally collected data.

In the second part, the analysis of how the performance of the multichannel equalizer of time-varying underwater acoustic communication channels depends on the number of sensors and the separation between them is presented. While the sensors in a conventional MIMO system need to be sufficiently apart so that the signals at their outputs are uncorrelated, conventional wisdom is that array processing applications require that sensors be separated by no more than one half of the shortest wavelength of the received signals. However, the selection of optimal sensor separation is a more subtle problem in the context of underwater acoustic communications. To study this problem, we introduce an arrival model which accounts for wideband and spatially spread nature of the received underwater acoustic communication signals. Using a particular arrival structure, we show that the performance is optimized for a finite separation between sensors which is not necessarily equal to one half of the shortest wavelength of the received signal. Also, an intuition behind this behavior is presented.

Appendix
Derivation of (44)

A crucial point in our analysis is the observation that the LS-based adaptation of the equalizer's coefficients $\mathbf{w}(n)$ can be framed as a channel identification problem, where an unknown channel is the MMSE filter $\mathbf{w}_{\mathrm{MMSE}}$ which processes the input $\mathbf{u}(n)$ and whose output is corrupted with a white noise process $q(n)$ of the power σ^2_{MMSE}, such that a sequence of transmitted symbols $x(n)$ is produced, i.e.,

$$x(n) = \mathbf{w}^H_{\mathrm{MMSE}}\mathbf{u}(n) + q(n). \tag{34}$$

Intuitively, as the number of observation vectors $\mathbf{u}(n)$ grows, the equalizer weight vector $\mathbf{w}(n)$ approaches that of the MMSE equalizer. Consequently, we view the DFE equalizer as an adaptive processor which is "trying" to get as close as possible to the MMSE processor. Since the statistics of the received process are unknown and estimated using time-domain averaging, the DFE equalizer behaves as an adaptive processor which estimates the MMSE processor based on the received signal and the desired output.

Therefore, a signal prediction error $\xi(n)$ uses (5) and (34) expressed as

$$\begin{aligned}\xi(n) &= x(n) - \hat{x}_{\mathrm{soft}}(n)\\ &= \boldsymbol{\epsilon}^H(n-1)\underline{\tilde{\mathbf{u}}}(n) + q(n)\end{aligned} \tag{35}$$

where

$$\boldsymbol{\epsilon}(n) = \mathbf{w}_{\mathrm{MMSE}} - \mathbf{w}(n) \tag{36}$$

measures how far the estimated equalizer weight vector $\mathbf{w}(n)$ is from the optimal (MMSE) equalizer $\mathbf{w}_{\mathrm{MMSE}}$. We refer to it as an equalizer estimation error.

Since the noise process $q(n)$ is uncorrelated with the received signal $\mathbf{u}(n)$ and equalizer estimation error $\boldsymbol{\epsilon}(n-1)$, the signal prediction MSE is, therefore, given by

$$\mathbf{E}\left[|\boldsymbol{\xi}(n)|^2\right] = \mathbf{E}\left[\boldsymbol{\epsilon}^H(n-1)\mathbf{u}(n)\mathbf{u}^H(n)\boldsymbol{\epsilon}(n-1)\right] + \sigma^2_{\mathrm{MMSE}}. \tag{37}$$

Using the facts that $\mathrm{tr}\{\mathbf{AB}\} = \mathrm{tr}\{\mathbf{BA}\}$, for square matrices $\mathbf{A}$ and $\mathbf{B}$, and that the expectation and trace operators commute, the signal prediction MSE is further given by

$$\begin{aligned}&\mathbf{E}\left[|\boldsymbol{\xi}(n)|^2\right]\\ &= \mathrm{tr}\left\{\mathbf{E}\left[\mathbf{u}(n)\mathbf{u}^H(n)\boldsymbol{\epsilon}(n-1)\boldsymbol{\epsilon}^H(n-1)\right]\right\} + \sigma^2_{\mathrm{MMSE}}.\end{aligned} \tag{38}$$

Assuming that the received signal $\mathbf{u}(n)$ at time n and the equalizer estimation error $\boldsymbol{\epsilon}(n-1)$ at time $n-1$ are uncorrelated, the signal prediction MSE is expressed as

$$\mathbf{E}\left[|\boldsymbol{\xi}(n)|^2\right] = \mathrm{tr}\left\{\mathbf{R}\mathbf{E}\left[\boldsymbol{\epsilon}(n-1)\boldsymbol{\epsilon}^H(n-1)\right]\right\} + \sigma^2_{\mathrm{MMSE}} \tag{39}$$

where $\mathbf{R}$ is the ensemble correlation matrix of the received process, defined in (9). Note that the first term in (39) is the signal prediction excess error. It appears because the number of

symbols used to train the equalizer's coefficients is finite. The analysis from here on assumes finite n but that $\lambda = 1$.

The equalizer estimation error $\boldsymbol{\epsilon}(n)$ can be expressed using (34) and (13) as

$$\begin{aligned}\boldsymbol{\epsilon}(n) &= \mathbf{w}_{\mathrm{MMSE}} - \hat{\mathbf{R}}^{-1}(n)\hat{\mathbf{r}}(n) \\ &= \mathbf{w}_{\mathrm{MMSE}} - \hat{\mathbf{R}}^{-1}(n)\sum_{i=1}^{n}\mathbf{u}(i)\left(\mathbf{u}^H(i)\mathbf{w}_{\mathrm{MMSE}} + q^*(i)\right) \\ &= -\hat{\mathbf{R}}^{-1}(n)\sum_{i=1}^{n}\mathbf{u}(i)q^*(i). \end{aligned} \tag{40}$$

A correlation matrix of the equalizer estimation error uses (40) evaluated as

$$\begin{aligned}\mathbf{E}\left[\boldsymbol{\epsilon}(n)\boldsymbol{\epsilon}^H(n)\right] &= \mathbf{E}\left[\hat{\mathbf{R}}\sum_{i=1}^{n}\mathbf{u}(i)q^*(i)\sum_{j=1}^{n}q(j)\mathbf{u}^H(j)\hat{\mathbf{R}}\right] \\ &= \sigma^2_{\mathrm{MMSE}}\mathbf{E}\left[\hat{\mathbf{R}}^{-1}(n)\right] \end{aligned} \tag{41}$$

where the last equality follows from the fact that noise process $q(i)$ is white and uncorrelated with the received signal $\mathbf{u}$.

To proceed further, we employ the results which characterize the expectation of the SCM inverse. The expectation of the SCM inverse is evaluated using the random matrix theory results, as elaborated on in [20]. Namely, if the order of the SCM m and the number of observations n grow large at the same rate such that $m/n \to c \in (0, 1)$, the expected inverse of the SCM converges such that

$$\mathbf{E}\left[\hat{\mathbf{R}}^{-1}(n)\right] \to \frac{\mathbf{R}^{-1}}{n-m}. \tag{42}$$

Due to a rapid convergence, the asymptotic result fairly accurately approximates the finite m and n case such that

$$\mathbf{E}\left[\hat{\mathbf{R}}^{-1}(n)\right] \approx \frac{\mathbf{R}^{-1}}{n-m}. \tag{43}$$

Substituting (43) into (41) and the obtained result into (39) yields an approximation for the signal prediction MSE

$$\mathbf{E}\left[|\xi(n)|^2\right] \approx \frac{n-1}{n-(NL_{\mathrm{ff}}+L_{\mathrm{fb}})-1}\sigma^2_{\mathrm{MMSE}} \tag{44}$$

which is valid for $n > NL_{\mathrm{ff}} + L_{\mathrm{fb}} + 1$. We note that (44) holds exactly if the received signal is Gaussian, which happens when the transmitted signal is Gaussian itself and/or the transmission channels $\mathbf{g}_i$ are long enough such that their outputs are approximately Gaussian by the central limit theorem [20].

REFERENCES

[1] B. Sklar, "Rayleigh fading channels in mobile digital communication systems—Part I: Characterization," *IEEE Commun. Mag.*, vol. 35, no. 7, pp. 90–100, Jul. 1997.

[2] M. Stojanovic and J. C. Preisig, "Underwater acoustic communication channels: Propagation models and statistical characterization," *IEEE Commun. Mag.*, vol. 47, no. 1, pp. 84–89, Jan. 2009.

[3] B. Sklar, "Rayleigh fading channels in mobile digital communication systems—Part II: Mitigation," *IEEE Commun. Mag.*, vol. 35, no. 7, pp. 102–109, Jul. 1997.

[4] A. C. Singer, J. K. Nelson, and S. S. Kozat, "Signal processing for underwater acoustic communications," *IEEE Commun. Mag.*, vol. 47, no. 1, pp. 90–96, Jan. 2009.

[5] J. C. Preisig, "Performance analysis of adaptive equalization for coherent acoustic communications in the time-varying ocean environment," *J. Acoust. Soc. Amer.*, vol. 118, pp. 263–278, Jul. 2005.

[6] D. Gesbert, M. Shafi, D. Shiu, P. J. Smith, and A. Naguib, "From theory to practice: An overview of MIMO space-time coded wireless systems," *IEEE J. Sel. Areas Commun.*, vol. 21, no. 3, pp. 281–302, Apr. 2003.

[7] H. L. V. Trees, *Optimum Array Processing: Detection, Estimation and Modulation Theory*. New York, NY, USA: Wiley, 2002, ch. 2.

[8] N. Al-Dhahir and J. M. Cioffi, "MMSE decision-feedback equalizers: Finite-length results," *IEEE Trans. Inf. Theory*, vol. 41, no. 4, pp. 961–975, Jul. 1995.

[9] N. Al-Dhahir and A. H. Sayed, "The finite-length multi-input multi-output MMSE-DFE," *IEEE Trans. Signal Process.*, vol. 48, no. 10, pp. 2921–2936, Oct. 2000.

[10] Y. Gong and C. F. N. Cowan, "Optimum decision delay of the finite-length DFE," *IEEE Signal Process. Lett.*, vol. 11, no. 11, pp. 858–861, Nov. 2004.

[11] Y. Gong and C. F. N. Cowan, "A self structured adaptive decision feedback equalizer," *IEEE Signal Process. Lett.*, vol. 13, no. 3, pp. 169–172, Mar. 2006.

[12] M. Stojanovic, J. Catipovic, and J. Proakis, "Adaptive multichannel combining and equalization for underwater acoustic communications," *J. Acoust. Soc. Amer.*, vol. 94, no. 3, pp. 1621–1631, 1993.

[13] M. Stojanovic, J. Catipovic, and J. Proakis, "Reduced complexity spatial and temporal processing of underwater acoustic communication signals," *J. Acoust. Soc. Amer.*, vol. 98, no. 2, pp. 961–972, 1995.

[14] M. Stojanovic, "Efficient processing of acoustic signals for high rate information transmission over sparse underwater channels," *J. Phys. Commun.*, pp. 146–161, 2008.

[15] W. Xiao and M. L. Honig, "Large system transient analysis of adaptive least squares filtering," *IEEE Trans. Inf. Theory*, vol. 51, no. 7, pp. 2447–2474, Jul. 2005.

[16] M. J. M. Peacock, I. B. Collings, and M. L. Honig, "Unified large-system analysis of MMSE and adaptive least squares receivers for a class of random matrix channels," *IEEE Trans. Inf. Theory*, vol. 52, no. 8, pp. 3567–3600, Aug. 2006.

[17] J. Preisig, "Subarray partitioning for adaptive multichannel equalization," in *Proc. 11th Eur. Conf. Underwater Acoust.*, Jul. 2012, pp. 1698–1702.

[18] S. Haykin, *Adaptive Filter Theory*, 4th ed. Englewood Cliffs, NJ, USA: Prentice-Hall, 2002.

[19] A. Edelman, "Eigenvalues of random matrices," Notes from the MIT's Class 18.338, 2011.

[20] M. Pajovic, "The development and application of random matrix theory in adaptive signal processing in the sample deficient regime," Ph.D. dissertation, Massachusetts Inst. Technol./Woods Hole Oceanogr. Inst., Cambridge/Woods Hole, MA, USA, 2014.

[21] V. A. Marcenko and L. A. Pastur, "Distribution of eigenvalues in certain sets of random matrices," *Mat. Sb. (N.S.)*, vol. 72, no. 114, pp. 507–536, 1967.

[22] M. Pajovic and J. Preisig, "Performance analysis of the least squares-based multichannel decision feedback equalization of time-varying channels," in *Proc. IEEE Global Commun. Conf.*, 2013, pp. 3312–3317.

[23] W. Hodgkiss and J. Preisig, "Kauai ACOMMS MURI 2011 (KAM11) experiment," in *Proc. 11th Eur. Conf. Underwater Acoust.*, 2012, pp. 993–1000.

[24] M. Stojanovic, "On the relationship between capacity and distance in an underwater acoustic communication channel," *ACM SIGMOBILE Mobile Comput. Commun. Rev.*, vol. 11, no. 4, pp. 34–43, Oct. 2007.

[25] M. Hayes, *Statistical Digital Signal Processing and Modeling*. New York, NY, USA: Wiley, 1996, ch. 3.

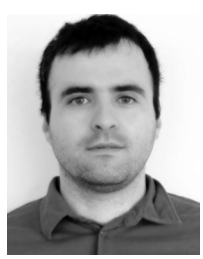

Milutin Pajovic received the B.S. degree in electrical engineering from the University of Montenegro, Podgorica, Montenegro, in 2005, the M.S. degree in ocean engineering from the Florida Atlantic University, Boca Raton, FL, USA, in 2009, and the Ph.D. degree in electrical and ocean engineering from the Massachusetts Institute of Technology/Woods Hole Oceanographic Institution Joint Program, Cambridge/Woods Hole, MA, USA, in 2014.

He worked as an Engineer for Communication Networks and Services at the Agency for Electronic Communications of Montenegro between 2005 and 2007. He is currently a member of the research

staff at the Mitsubishi Electric Research Laboratories, Cambridge, MA, USA. His research interests are in the areas of signal processing for physical-layer wireless and optical communications, array signal processing, random matrix theory, and machine learning.

James C. Preisig received the B.S. degree in electrical engineering from the U.S. Coast Guard Academy, New London, CT, USA, in 1980, the S.M. and E.E. degrees in electrical engineering from the Massachusetts Institute of Technology, Cambridge, MA, USA, in 1988, and the Ph.D. degree in electrical and ocean engineering from the Massachusetts Institute of Technology/Woods Hole Oceanographic Institution (WHOI) Joint Program in Oceanography and Oceanographic Engineering in 1992.

He served on active duty in the Coast Guard until August 1985. He was a Postdoctoral Investigator at WHOI from 1992 to 1994 and a Visiting Assistant Professor at Northeastern University, Boston, MA, USA, from 1994 to 1997. From July 1997 through November 2014, he was a member of the scientific staff of the Department of Applied Ocean Physics and Engineering at WHOI and received Tenure in August 2005. He retired in November 2014 and currently holds an Emeritus Scientist appointment in that department. He founded JPAnalytics LLC, Falmouth, MA, USA, in September 2013, a small business focused on developing innovative signal modeling, analysis, and processing techniques that address challenging signal processing problems. His research interests are in the areas of adaptive signal processing, system identification, underwater acoustic propagation modeling, underwater acoustic communications and array processing, numerical optimization, and the development of embedded signal processing systems.

Dr. Preisig is the recipient of the 1999 Office of Naval Research Ocean Acoustics Young Faculty Award and is a Fellow of the Acoustical Society of America (ASA). He is a member of the ASA's Underwater Acoustics and Signal Processing Technical Committees and currently serves on the ASA's Membership Committee. He has served as an Associate Editor of the IEEE JOURNAL OF OCEANIC ENGINEERING and as a member of the IEEE Sensor Array and Multichannel Signal Processing Technical Committee.